AGU PUBLICATIONS

JGR

Journal of Geophysical Research: Space Physics

RESEARCH ARTICLE

10.1002/2014JA020809

Key Points:
- Bending arcs are dayside polar cap arcs
- Bending arcs are ionospheric signatures of pulsed dayside reconnection
- Bending arcs occur along open field lines

Correspondence to:
J. A. Carter,
jac48@leicester.ac.uk

Citation:
Carter, J. A., S. E. Milan, R. C. Fear, A. Kullen, and M. R. Hairston (2015), Dayside reconnection under interplanetary magnetic field B_y-dominated conditions: The formation and movement of bending arcs, *J. Geophys. Res. Space Physics*, *120*, doi:10.1002/2014JA020809.

Received 19 NOV 2014
Accepted 2 MAR 2015
Accepted article online 6 MAR 2015

Dayside reconnection under interplanetary magnetic field B_y-dominated conditions: The formation and movement of bending arcs

J. A. Carter[1], S. E. Milan[1], R. C. Fear[1,2], A. Kullen[3], and M. R. Hairston[4]

[1]Department of Physics and Astronomy, University of Leicester, Leicester, UK, [2]Now at School of Physics and Astronomy, University of Southampton, Southampton, UK, [3]Department of Space and Plasma Physics, KTH Royal Institute of Technology, Stockholm, Sweden, [4]William B. Hanson Center for Space Sciences, University of Texas at Dallas, Richardson, Texas, USA

Abstract Based upon a survey of global auroral images collected by the Polar Ultraviolet Imager, Kullen et al. (2002) subdivided polar cap auroral arcs into a number of categories, including that of "bending" arcs. We are concerned with those bending arcs that appear as a bifurcation of the dayside auroral oval and which subsequently form a spur intruding into the polar cap. Once formed, the spur moves poleward and antisunward over the lifetime of the arc. We propose that dayside bending arcs are ionospheric signatures of pulses of dayside reconnection and are therefore part of a group of transient phenomena associated with flux transfer events. We observe the formation and subsequent motion of a bending arc across the polar cap during a 30 min interval on 8 January 1999, and we show that this example is consistent with the proposed model. We quantify the motion of the arc and find it to be commensurate with the convection flows observed by both ground-based radar observations and space-based particle flow measurements. In addition, precipitating particles coincident with the arc appear to occur along open field lines, lending further support to the model.

1. Introduction

Polar cap arcs are structured regions of enhanced auroral emission within the normally dark area of the polar cap. The polar cap is spatially bounded by the auroral oval and encompasses the region of open magnetic flux where the Earth's magnetic field is linked to the interplanetary medium. Polar cap arcs, including transpolar arcs (TPAs) are auroral features that are seen to significantly protrude into the polar cap region, in some cases even extending all the way from the nightside to the dayside [*Frank et al.*, 1982].

Polar cap arcs form predominantly during periods of northward interplanetary magnetic field (IMF) [*Berkey et al.*, 1976; *Gussenhoven*, 1982] and tend to be roughly aligned parallel to the noon-midnight meridian, such that they are sometimes known as Sun-aligned arcs. Once formed, an arc may remain stationary or move dawnward or duskward, sometimes reversing in direction, before eventually disappearing. The initial location of the formation of the arc, in magnetic local time, has been shown to be influenced by the B_y component of the IMF. *Gussenhoven* [1982] found that an arc will preferentially form in the postmidnight sector in the Northern Hemisphere when IMF $B_y < 0$ nT or premidnight when $B_y > 0$ nT. The formation location is observed in the opposite sense for arcs detected in the Southern Hemisphere [*Gusev and Troshichev*, 1986].

The dependence on IMF B_y orientation of the formation of TPAs has been shown to be consistent with models invoking a twisted magnetotail [*Kullen and Janhunen*, 2004, and references therein], some of which involve magnetic reconnection [*Milan et al.*, 2005]. These models have been comprehensively reviewed by *Fear and Milan* [2012a]. The location of the nightside transpolar arc in the cases presented in *Fear and Milan* [2012a] is shown to be correlated with the IMF B_y component at Earth (via the time-shifted OMNI data set as described in *King and Papitashvili* [2005]). This correlation is found to be strongest with the IMF B_y component several hours before the arc forms. The separate physical processes and associated timescales governing the initial location and subsequent motion of transpolar arcs can explain the fact that arcs which cross from one side of the polar cap to the other are often associated with periods in which the sign of the IMF B_y component changes [*Fear and Milan*, 2012a], as previously observed [*Kullen et al.*, 2002]. In the *Milan*

et al. [2005] model, under northward IMF conditions and following a period of tail reconnection, a region of closed magnetic flux protrudes into the otherwise open polar cap at a local time that is reflected about the midnight meridian for each hemisphere. The tail reconnection also results in strong azimuthal ionospheric flows seen on the nightside auroral oval around the time of polar cap arc formation [*Milan et al.*, 2005; *Fear and Milan*, 2012b]. Although the formation of the arc in this model occurs as a response to reconnection in the magnetotail, the subsequent motion of the arc was shown to be due to "lobe" reconnection along the high-latitude magnetopause, which causes a redistribution of magnetic flux in the polar cap, known as lobe stirring. Once formed, the subsequent motion of the TPA is controlled by the sign and magnitude of the IMF B_y component, which controls the location of lobe reconnection on the magnetopause and hence the sense of lobe stirring. As lobe reconnection is distinct in each hemisphere, the motion of the TPA in one hemisphere is anticipated to be independent from the motion of the TPA in the opposite hemisphere. A recent case study of a TPA [*Fear et al.*, 2014], observed during a conjunction with the Cluster spacecraft, has demonstrated that closed magnetic flux is observed at high altitudes in the magnetotail, which moves to and fro as predicted by the *Milan et al.* [2005] mechanism.

The present paper is concerned with a particular category of polar cap arc, that of "bending arcs." A comprehensive survey of the occurrence and motion of polar cap arcs over a 3 month period was undertaken by *Kullen et al.* [2002] using Polar Ultraviolet Imager (UVI) images of the Northern Hemisphere auroras. This study sorted all the detected polar arcs within their data set into five separate categories, based on the arcs' morphology: oval-aligned, bending, moving, midnight, and multiple arcs. *Kullen et al.* [2002] define bending arcs as hook-shaped poleward moving arcs where the sunward end of the arc, the observable tip, separates from the main auroral oval. The tip can then move into the polar cap toward the other side of the oval, whereas in contrast, the oval-connected end, the base, remains almost stationary. This paper is concerned only with those bending arcs that form primarily on the dayside of the polar cap (the base of the arc may start around dawn or dusk), from which the tip detaches from the dayside oval and moves poleward. This paper is not concerned with other hook-shaped arc phenomena reported in the literature (as cautioned by *Kullen* [2012] and, for example, as shown in *Fear and Milan* [2012b, Figure 3] or *Ismail and Meng* [1982], which although both fit the general *Kullen et al.* [2002] description of a bending arc are not dealt with in this paper). The *Fear and Milan* [2012b] case can be adequately explained using the *Milan et al.* [2005] model, as is evident by the observed requisite nightside reconnection flows in the data, but this model is unable to explain the cases of dayside bending arcs which are the focus of this paper. *Kullen et al.* [2002] reported that bending arcs occur predominantly when IMF $|B_y| > |B_z|$. In the *Kullen et al.* [2002] survey, they occurred predominantly near dawn or dusk. *Kullen et al.* [2002] also noted that an "oval-aligned" arc (an almost stationary auroral feature that stretches across the auroral oval but positioned considerably dawnward or duskward) is often seen simultaneously to a bending arc close to the opposite auroral oval side. *Kullen et al.* [2002] found that bending arcs are short lived, disappearing from the polar cap within 1 h, in contrast with other types which often persist for longer. In the *Kullen et al.* [2002] study 22 out of 74 total events were classified as bending arcs.

Kullen et al. [2002] found that bending arcs have characteristics that differ considerably from the other classes of polar cap arcs: they appear largely on the dayside, they form when the IMF is B_y dominated rather than when $B_z > 0$ nT, and they move largely antisunward rather than dawnward or duskward. Moreover, *Kullen et al.* [2002] concluded that most bending arcs start to develop in the opposite side of the auroral oval to the usual IMF B_y dependence of polar cap arcs. In a more recent study (Kullen et al., manuscript in preparation, 2015), the authors show that the IMF B_z component is close to zero for nearly all the bending arc cases (so that the IMF B_y component dominates). In addition, out of the 22 bending arc cases presented by Kullen et al. (manuscript in preparation, 2015), 17 occur on the dayside of the polar cap. We will argue that these characteristics are consistent with a formation mechanism that depends on magnetopause rather than magnetotail reconnection. We propose a model that explains the evolution of the bending arc from its formation within the dayside of the polar cap, during its poleward and antisunward movement across the polar cap, on to its inevitable destruction following a change in the rates of dayside and nightside reconnection.

This paper is laid out as follows. In section 2 we present an example observation of a bending arc. We also examine the solar wind parameters that occurred at the time of this observation, and we show ground-based radar measurements of the polar cap and precipitating particle fluxes obtained from an in

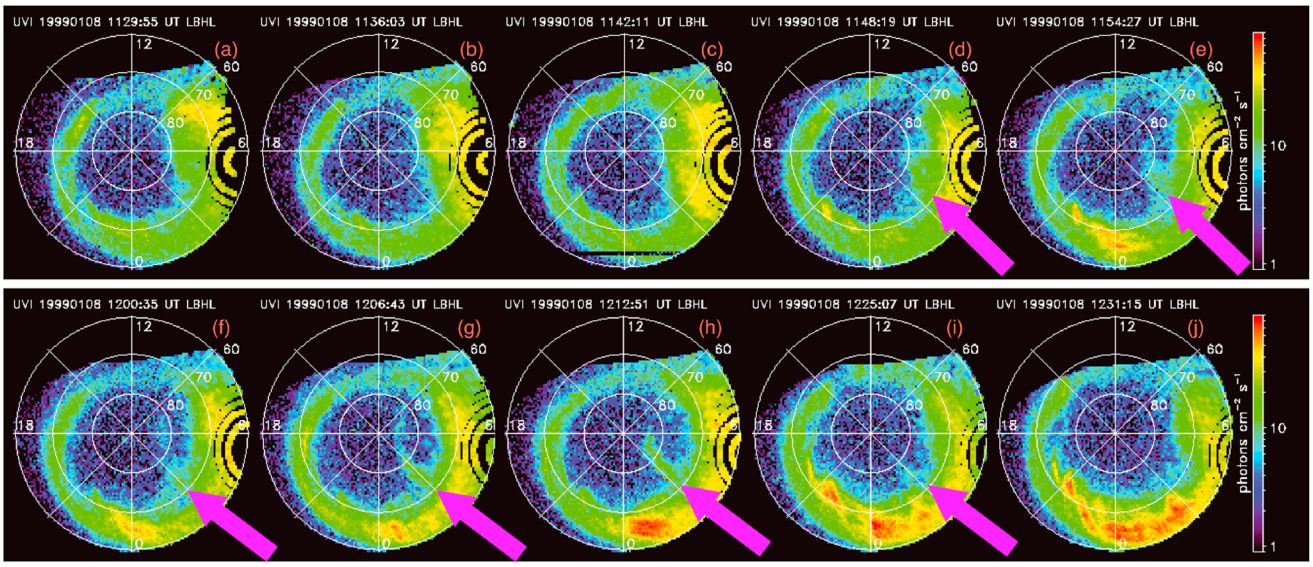

Figure 1. UV images (LBHl band images with an integration time of 36 s) from the Polar spacecraft showing the example bending arc crossing the polar cap. The position of the base of the bending arc is marked by the pink arrows. Noon is toward the top, and dawn is to the right for each image. The black concentric circles in the dawn sector of the images result from the projection of the data from Polar's location as it moves in its orbit, onto a magnetic latitude-longitude grid.

situ spacecraft. In section 3 we test the example observation in light of a model of bending arcs, and we finish with our conclusions in section 4.

2. Observations

The observation chosen to illustrate the bending arc mechanism was taken on 8 January 1999 by the UVI instrument on board the Polar spacecraft [*Torr et al.*, 1995]. The UVI instrument measured auroral emission using four narrowband filters. Two of these filters covered the Lyman-Birge-Hopfield band that results from electron impact excitation of N_2. These filters were centered on 1700 and 1500 Å (LBHl (Lyman-Birge-Hopfield long filter) and LBHs (Lyman-Birge-Hopfield short filter) bands, respectively). The example observation used in this paper is listed in the set of *Kullen et al.* [2002] and is illustrated in Figure 1. *Kullen et al.* [2002] used the LBHl filter UV images in their study to avoid atmospheric absorption effects (and so the intensity of the emission is nearly directly proportional to the electron energy flux impinging on the ionosphere). A bending arc was identified that was visible between 11:48 UT and 12:25 UT. This particular observation was taken for further study as concurrent measurements taken by the Super Dual Auroral Radar Network (SuperDARN) [*Greenwald et al.*, 1995; *Chisham et al.*, 2007] and high-latitude passes of the DMSP spacecraft [*Hardy et al.*, 1984] enabled the associated ionosphere convection and particle precipitation to be considered.

2.1. Images of the Arc

In Figure 2 we plot a sequence of images from the Polar UVI LBHs filter of the example bending arc. We only plot images with exposure times of 36 s. In these same images we superimpose SuperDARN convection patterns and lines of electrostatic equipotential. These patterns are discussed in more detail in section 2.3 below. The bending arc forms in the brightest region of the morning sector, as seen at 11:49 UT (Figures 2b or 1d at UT 11:48). The base of the bending arc moves slowly antisunward over the course of the sequence, toward its disappearance after 12:26 UT. The base of the arc ends in the 2 magnetic local time (MLT) sector (Figures 2h or 1i at UT 12:25). The tip of the bending arc, after detaching from the main auroral oval, also moves but at a different rate to the base and moves poleward (Figures 1e–1g). The poleward tip is first noted in the 8 MLT sector but terminates within the 3 MLT sector (Figures 2b–2g or Figures 1e–1h). We discuss the motion of the arc in more detail in section 3. Throughout this sequence, the auroral oval remains fairly constant in size and almost static in location, despite the nightside brightenings in the latter half of the period.

2.2. Solar Wind and Geomagnetic Activity

Figure 3 shows the solar wind parameters during the beginning part of the day under study, as measured by the Advanced Composition Explorer (ACE) at the Sun-Earth Lagrangian point L1 (~240 R_E upstream of

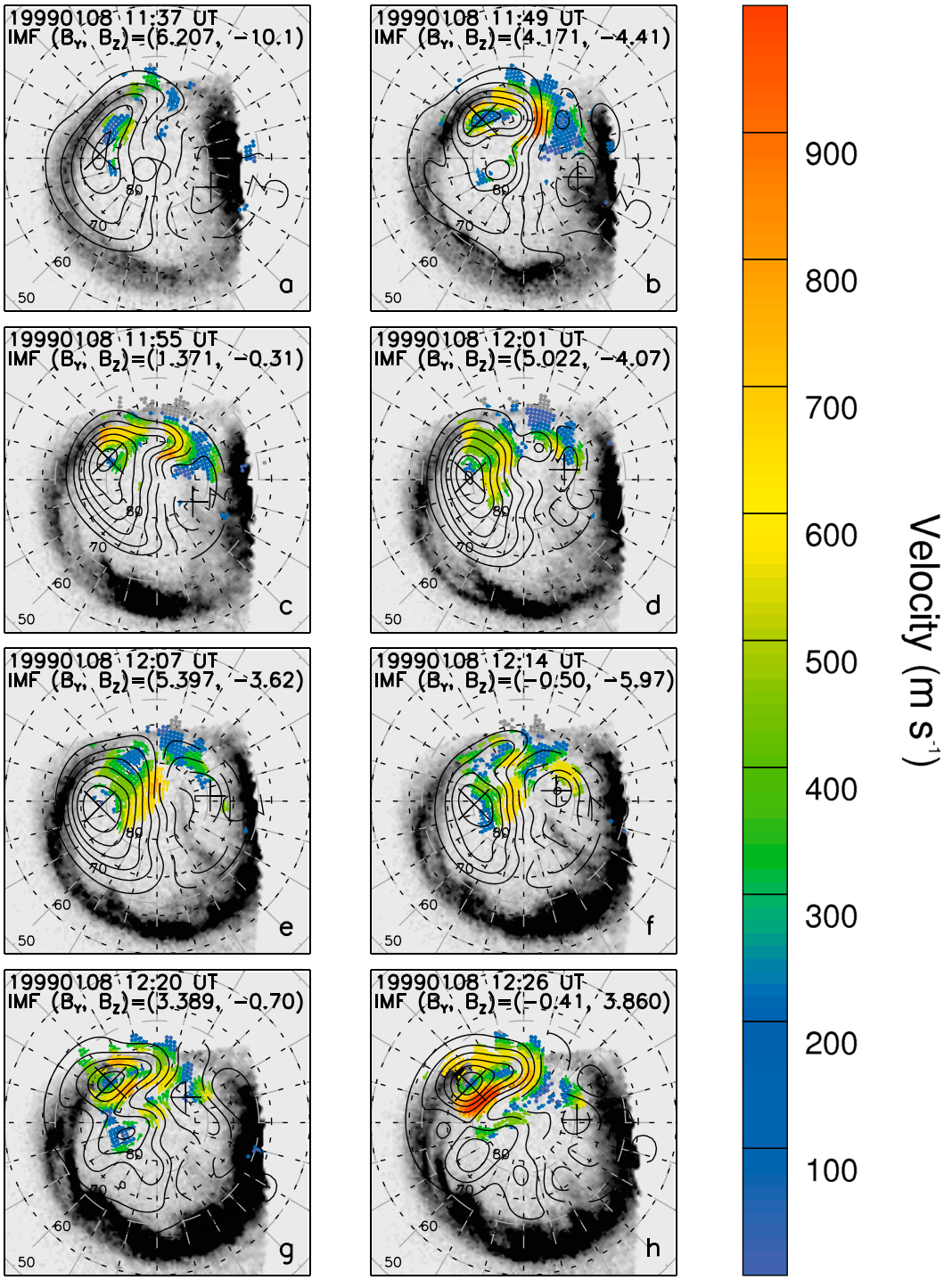

Figure 2. Sequences of images obtained from Polar (LBHs filter), showing the progression of the bending arc in the Northern Hemisphere between 11:36 and 12:26 UT. We also note the IMF B_y and B_z values (from Wind). Superimposed on each image are flows obtained by SuperDARN radar, along with the calculated electrostatic potential pattern. Noon is toward the top, and dawn is to the right for each image.

Earth) and lagged to their arrival at the subsolar bow shock. The ACE data were accessed via the OMNI data set. Although the OMNI data set, as a whole, is made up of a combination of data obtained from multiple spacecraft which is subsequently lagged appropriately for travel time to the Earth, our period of interest consisted solely of data taken by the ACE satellite. We also include a trace of the solar wind parameters as

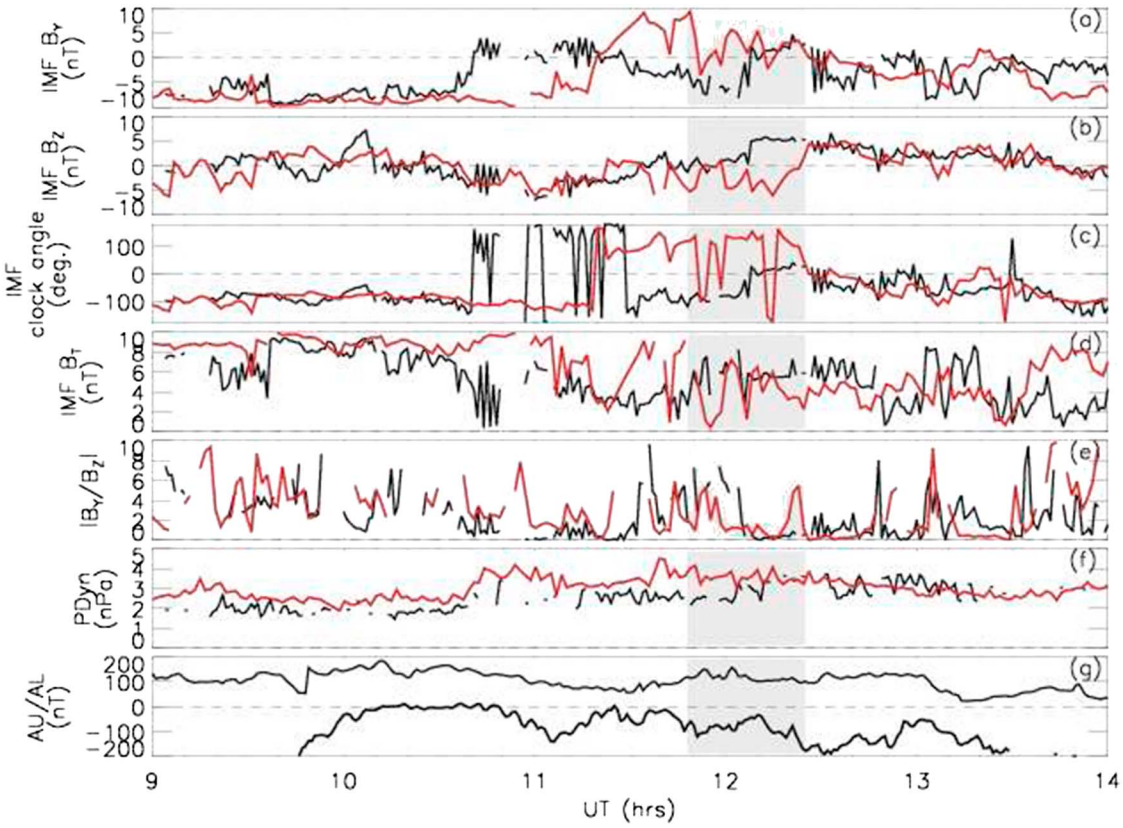

Figure 3. Solar wind and geomagnetic conditions during the period of interest. (a–f) Solar wind conditions are given. In Figures 3a and 3b we plot the IMF B_y and B_z components, respectively. In Figure 3c we plot the IMF clock angle. In Figure 3d we plot the magnitude of the IMF (for the combined B_y and B_z components). In Figure 3e we plot the ratio of B_y to B_z. In Figure 3f we plot the solar wind dynamic pressure. Data obtained from both OMNI (black) and Wind (red) are plotted. (g) We plot the geomagnetic indices *AU* (upper trace) and *AL* (lower trace). The period when the arc was visible is highlighted in grey in each panel.

measured by Wind on the same axes. At the time of the bending arc, Wind was found slightly upstream of the bow shock at a position with a GSE_X coordinate of 19.8 R_E compared to the bow shock subsolar standoff distance of 14.4 R_E, found via *Khan and Cowley* [1999]. The GSE_Y coordinate of Wind was −70.7 R_E, and so the distance between Wind and ACE is large. We have lagged the Wind data by 1.1 min to account for the delay to the bow shock. The traces in Figure 3 show a complicated period of solar wind data with considerable discrepancies between the OMNI and Wind data sets. The period when the bending arc was visible is marked by the highlighted area in the figure. Wind is closer to the Earth than ACE; hence, for a period of complicated IMF we expect less error on the delay calculated between the Wind spacecraft and the bow shock than for a similar delay applied to the ACE data. As the IMF B_z component is primarily southward (shown in Figure 3), magnetic reconnection would have occurred at the dayside magnetopause during the entire period of the arc's lifetime.

From 11:30 UT, ~20 min before the arc appears, IMF $B_z \approx 0$ nT but dips southward several times (with a greater magnitude in the Wind data). The Wind data show B_z to be almost entirely southward for the lifetime of the arc but turning northward at the end of the arc's lifetime. The OMNI and Wind data show very different values of the IMF B_y component during the lifetime of the arc. Whereas the OMNI data give a mainly negative B_y component during the first half of the arc but turning positive in the latter half, the Wind data show B_y to be mainly positive with several short excursions to below zero throughout this period. However, for both the OMNI and Wind data sets, B_y dominates B_z for the first half of the lifetime of the arc ($|B_y|/|B_z| \simeq 6$ or 4 for OMNI and Wind, respectively). This is illustrated via the IMF clock angle and the ratio of IMF B_y to B_z, found in Figures 3c and 3e, respectively. For the second half of the arc's lifetime, the magnitudes are comparable, except for dominant B_y for a short period before the disappearance of the arc in the Wind data.

The solar wind dynamic pressure is low throughout the period of interest (for both OMNI and Wind), with no significant pulses or enhancements observed. A negative bay is seen in the *AL* index, shown by the lower

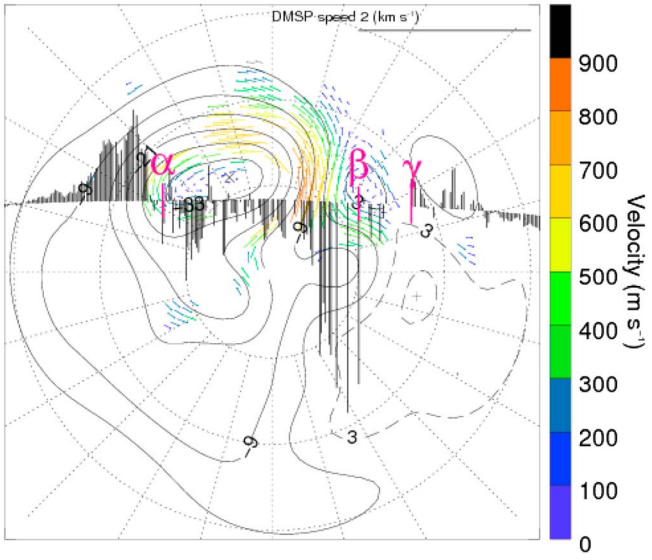

Figure 4. The orbit track of the DMSP F13 satellite, along with vectors representing the cross-track velocity, superimposed onto a snapshot of the plasma flows and the equipotential pattern obtained from SuperDARN data (colored arrows, shown at 11:46 UT). The DMSP data are plotted for times between 11:36 and 11:54 UT, and the satellite moved from the dusk to the dawn sector (left to right in the image). Noon is toward the top of the image. Positions of interest are marked and annotated in pink. These positions correspond to the annotations of Figure 5.

trace in the lowest panel of the figure. This indicates the commencement of a substorm which is consistent with the brightening seen in the nightside auroral oval in the latter panels of Figures 1 and 2.

2.3. DMSP and SuperDARN Observations

In Figure 4 we plot the DMSP track (F13 satellite of the DMSP suite) and the cross-track velocities, over a representative SuperDARN map from 11:46 UT. SuperDARN vectors are seen only on the dayside, but these are consistent with a twin-cell convection pattern, with a significant dawn-dusk asymmetry, with dawnward flows across the noon-midnight meridian and rapid flow into the polar cap in the prenoon sector. Flows such as these are signatures of low-latitude reconnection at the dayside magnetopause. These flows are consistent with the DMSP cross-track flows. Figure 2 shows that these fast flows into the polar cap are first observed between 11:37 and 11:49 UT, the period in which the bending arc is seen to separate from the morning sector auroral oval.

In Figure 5 we plot a spectrogram of precipitating ions and electrons as measured by the DMSP F13 satellite during the same pass (Figures 5a and 5b for ions and electrons, respectively). In Figure 5c we show an image of the polar cap from the Polar spacecraft and superimpose the DMSP orbital track on this image. The spacecraft moves from left to right in this image. We highlight the particular times of interest, which are annotated on each panel. We consider significant fluxes of >1 keV electrons to be the signature of magnetospheric plasma trapped on closed field lines. Position α marks when the population of precipitating electrons is seen to drop to lower energies in Figure 5b, which coincides with the ingress of the spacecraft across the open-closed field line boundary into the polar cap in Figure 5c. Position γ marks when the precipitating electrons return to a higher-energy population as the spacecraft crosses from the open to the closed field line region. The region demarcated by β and γ is a region of intense low-energy electrons and high-energy ions, which are consistent with magnetosheath population or cusp ion precipitation, i.e., precipitation on newly opened field lines. The positions of α, β, and γ are also marked in Figure 4, where the DMSP track between α and γ encompasses the antisunward flow in the open field line region. We discuss the particle precipitation further in section 3.

3. Discussion

We have presented an interval of data in which an auroral arc forms across the dawnside auroral oval and that subsequently moves into the polar cap. This feature has previously been identified as belonging to a category of polar cap arc, termed bending arcs [*Kullen et al.*, 2002]. Our observations show that the formation of the arc is associated with a rotation of the IMF to a B_y-dominated orientation, a characteristic feature of bending arcs (Kullen et al., manuscript in preparation, 2015). The associated ionospheric convection pattern, observed by SuperDARN and DMSP, shows dawn-dusk asymmetry consistent with a strongly B_y-dominated IMF orientation. Antisunward flows are colocated with the tip of the forming arc in a region of magnetosheath-like particle precipitation. We were fortunate to find an example of such an arc during a period of good SuperDARN observations and a fortuitous DMSP overpass. This combination of observations

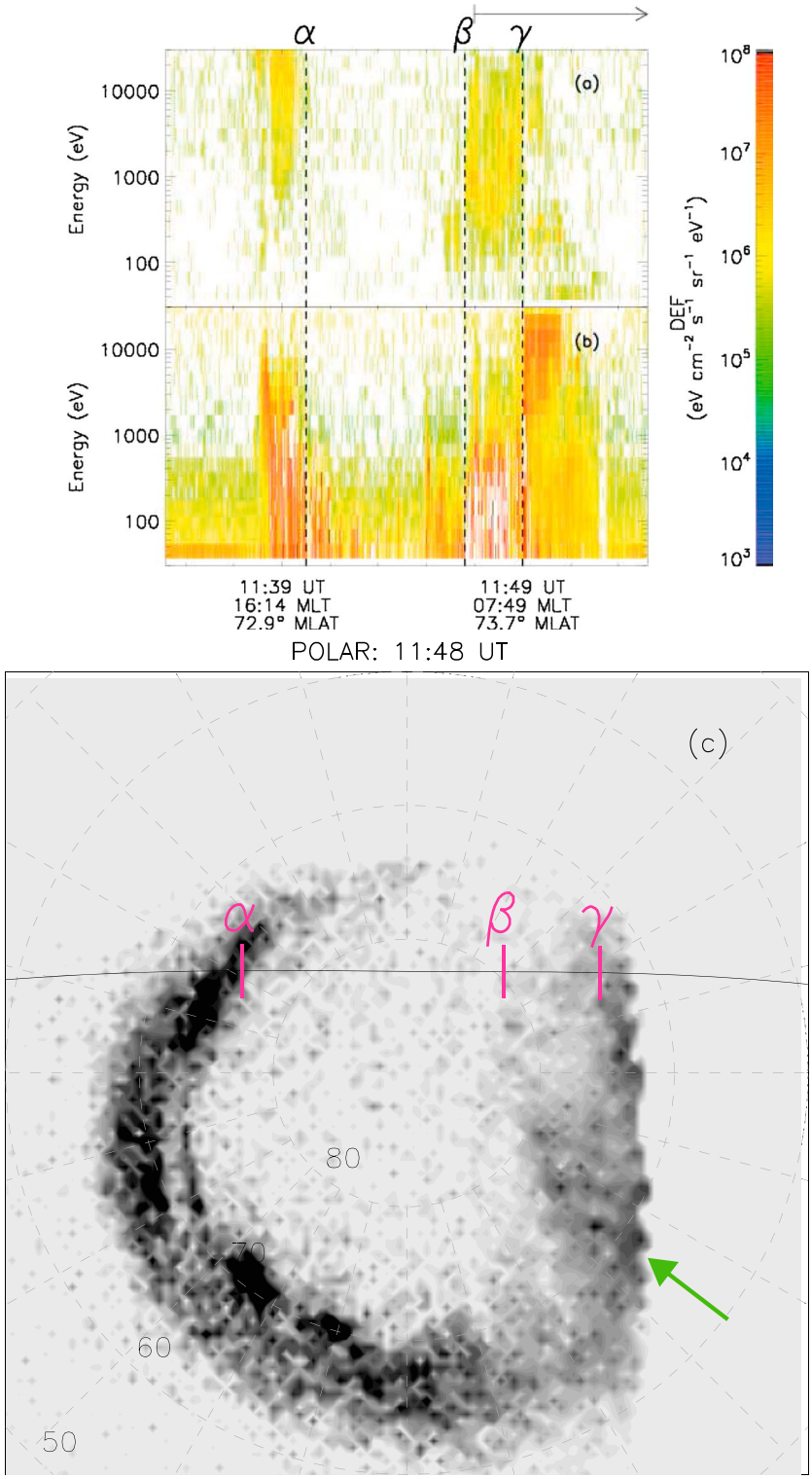

Figure 5. Spectrograms of (a) ions and (b) electrons as detected by the DMSP F13 satellite during the Northern Hemisphere high-latitude pass at the time of the bending arc. (c) We superimpose the satellite track on top of an image from Polar (LBHs filter). Times of interest are marked in all panels, by the dotted lines (Figures 5a and 5b) or positions marked in pink (Figure 5c). The arrow above Figure 5a denotes the start and continuation of the bending arc in time (which extends beyond this plot). The green arrow in Figure 5c marks the base of the arc.

suggests that the arc is associated with low-latitude magnetopause reconnection, and hence, its formation is similar to poleward moving auroral forms [*Fasel*, 1995; *Yeoman et al.*, 1997; *Milan et al.*, 2000; *Sandholt and Farrugia*, 2007] but occurring under B_y-dominated conditions.

In this section we examine the appearance and motion of the bending arc during its lifetime. The base and the tip of the arc, once formed, move at different rates within the polar cap. Our proposed scenario suggests that the newly opened field lines that constitute the arc are entrained within the background convection. Hence (later in this section), we compare these rates to the flow speeds from the convection patterns of SuperDARN and DMSP, in context of the IMF conditions.

The fast formation and response of the arc with reference to the contemporaneous solar wind conditions (as measured by Wind, as previously discussed) at the dayside magnetopause is in contrast to the delay expected between the upstream solar wind and the formation and response of the nightside TPA of the *Milan et al.* [2005] model, as observed by *Fear and Milan* [2012a]. TPAs (i.e., not bending arcs) in the *Milan et al.* [2005] model are postulated to occur on closed field lines. Therefore, bending arcs and other TPAs are phenomena that result from different mechanisms.

The DMSP spectrograms of Figure 5 show clear signatures of the main auroral oval in both the ion and electron plots, although this is perhaps clearer for the electrons. Hard ions and electrons, which we attribute to magnetospheric particle precipitation, are visible previous to the position α and post γ in Figures 5a and 5b, which correspond to the crossings of the satellite from a bright to a less bright region (α) or vice versa (γ). Some faint emission is visible during the crossing of the polar cap, as shown post α in the snapshot shown in Figure 5c, although it is much fainter than the emission seen along the main auroral oval. The energy of the electrons immediately post α is much lower than that of the main auroral oval (Figure 5b), and no significant signal in the detected ions at this time is observed. The period between β and γ also has considerable emission in Figure 5c, and this is the region in which the bending arc originates. Between β and γ higher fluxes of electrons and ions are observed in both spectrograms, as shown in Figures 5a and 5b, that exhibit softer energy spectra than those when crossing the main auroral oval, although at higher energies to those when traversing the main polar cap between α and β. We propose that the increase in electron fluxes in this period leads to the appearance of the UV emission seen as the bending arc. We attribute the emission and cusp ion signature observed to magnetosheath particles precipitating along newly opened field line following a burst of reconnection at the dayside magnetopause.

Flux transfer events (FTEs) manifest as a bifurcation of the auroral oval on similar timescales to bending arcs. Optical and radar emission is used to observe the quasiperiodic signatures of FTEs at the ionosphere [*Yeoman et al.*, 1997; *Milan et al.*, 1999a, 1999b, 2000; *Lockwood et al.*, 2001]. FTEs result from pulsed reconnection at the magnetopause during periods of southward IMF and have a recurrence rate of the order of 8 min [*Berchem and Russell*, 1984; *Rijnbeek et al.*, 1984]. The auroral signatures of FTE occur on newly opened field lines, as demonstrated by the detection of precipitating magnetospheric ions coincident with their emission signatures [*Lockwood et al.*, 2001]. The poleward moving auroral signatures of FTEs move eastward during periods of $B_y > 0$ nT [e.g., *Milan et al.*, 2000] in the Northern Hemisphere or westward for $B_y < 0$ nT, as would bending arcs. The bending arc we have observed formed during a single-pulse reconnection event resulting in the precipitation of particles from the magnetosheath into the dayside polar cap along open field lines.

The bending arc in this case forms adjacent to the open-closed field line boundary, as it occurs on newly opened field lines, which are by definition found next to this boundary. This scenario is illustrated schematically in Figure 6, and we describe each step of the scenario in turn in the following paragraph. This figure illustrates half the polar cap at two stages of the formation of the bending arc. Noon is toward the top of the image.

Following reconnection at the dayside magnetopause [*Dungey*, 1961, 1963], additional flux is added to the polar cap region (Figure 6a), as shown by the lilac area on the dayside polar cap. The occurrence of dayside reconnection is indicated by the combined observation sets of negative IMF B_z in Figure 3 and the strong dayside flows in Figure 2. The polar cap will accommodate the addition of open flux, and in the absence of nightside reconnection that closes flux, the main auroral oval will expand to lower latitudes [*Milan et al.*, 2012; *Cowley and Lockwood*, 1992]. The newly opened flux is found adjacent to the auroral oval (Figure 6b). The new flux will be found along the entire merging gap, as illustrated by the extended region of open flux

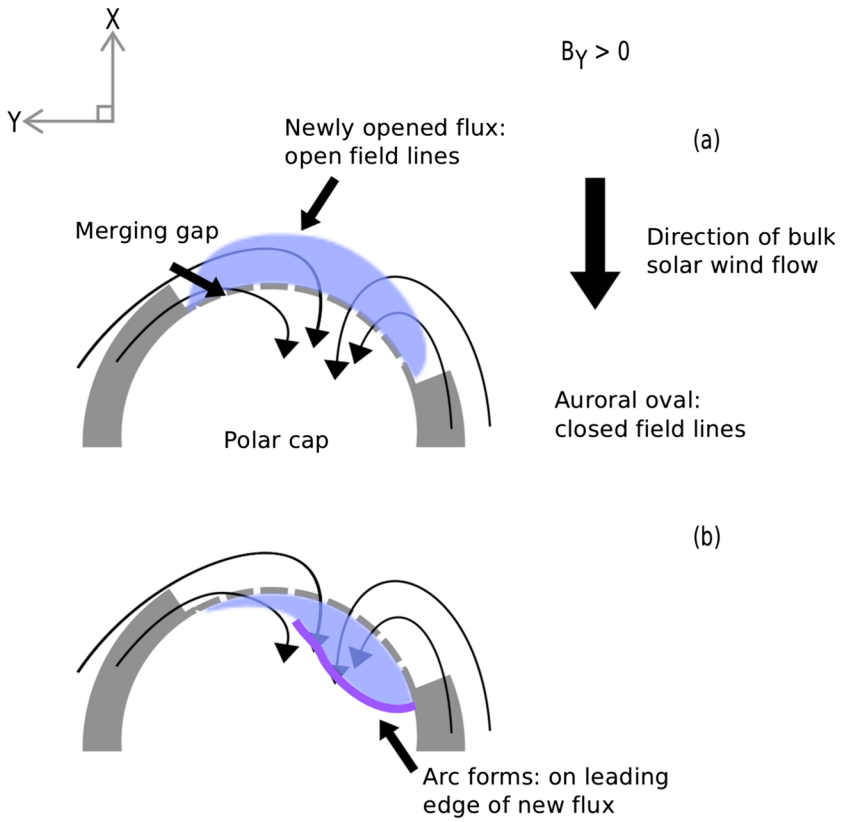

Figure 6. (a) Schematic of dayside reconnection and the addition of newly opened field lines to the polar cap, under IMF B_y-dominated conditions, (b) resulting in the formation of a bending arc on the leading edge (dark blue) of the open field line region. Only the dayside portion of the polar cap is shown. Noon is toward the top of each panel. Regions on newly opened field lines are shaded lilac. The main auroral oval is shown in grey.

including an area postnoon in Figure 6b. The dominant IMF B_y component in the illustrated case results in a strongly asymmetrical distribution of the newly added flux to the polar cap, via the highly skewed ambient convection pattern. The precipitation resulting in the auroral emissions of the bending arc occurs along the leading edge of the newly opened field lines, rather than along the closed field lines of the main auroral oval. As the newly open flux is incorporated into the polar cap by the ambient convection field (as indicated by the flow stream lines in the figure, consistent with the asymmetrical distribution of SuperDARN flows as shown in Figure 2), the bending arc breaks away from the auroral oval. The bulge of increased emission adjacent to the main auroral oval from which the bending arc "detaches," will be apparent providing there is a significant population of particles that can precipitate into the ionosphere that subsequently lead to observable auroral emissions. This picture is consistent with the observations of the precipitating particle signatures as measured by DMSP shown in Figure 5, as shown by the increase in electron fluxes as DMSP crosses over the region that result in the observable auroral signal of the bending arc.

Due to the transient nature of FTEs and given the mean recurrence rate of 8 min, a series of bending arcs might be expected to appear in the dayside polar cap. These bending arcs may become apparent if the number of precipitating particles exceeds the threshold required to produce observable auroral emissions. Dayside reconnection may cease, limiting the number of bending arcs observed. Additional dayside emission after the formation of the bending arc, resulting from a series of FTEs occurring on the dayside magnetopause, is not observed in our case. Instead, we observe the results of a single pulse of dayside reconnection. Any emission may be under the detection threshold of the Polar imager, or the recurrence rate for the FTEs during this period may be considerably longer than the mean recurrence rate, but well within the limits observed by *Berchem and Russell* [1984] or *Rijnbeek et al.* [1984].

The SuperDARN equipotential pattern is asymmetrical, and the largest cell appears in the dusk hemisphere (Figure 4). Such dayside flows are strongly azimuthal, coincident with the dayside auroral oval, consistent

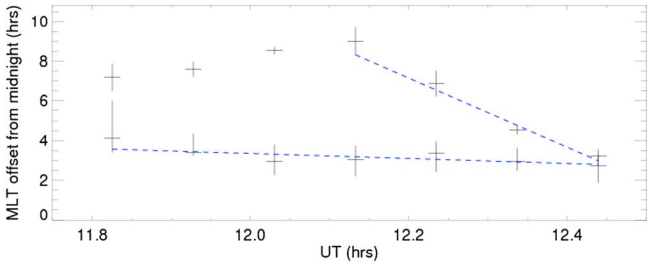

Figure 7. Movement of the bending arc, as shown by the offset in MLT position from midnight. An estimation of the error in the offset is shown by the upper and lower bounds of each point in the plot. In the lower trace we plot the motion of the base of the arc. In the upper trace we plot the motion of the tip of the arc. Linear fits to the traces or partial traces are plotted using a dashed blue line.

with the dominance of the positive B_y component (as observed in the Wind data). During the period under study, the measured SuperDARN flows occur primarily on the dawnside of the dayside auroral oval. This area is coincident with the dayside convection throat which maps to the site of reconnection at the magnetopause, with flows of the order of 900 m s^{-1} (for example, Figures 2d and 2e). There are no SuperDARN data points that sit near the base of the arc throughout the sequence (Figure 2). Therefore, we mainly concentrate our discussion on flows near the tip.

The motion of the bending arc is illustrated in Figure 7, by plotting the offset in MLT of the arc from midnight against time. In the bottom trace, the base of the arc can be seen to move a total of 0.77 h of MLT during a period of 37 min. We also plot a least squares linear fit to the relationship (blue dashed line), found by minimizing the χ^2 statistic. The motion is equivalent to a distance traveled of 418 km, assuming an average magnetic latitude at the base of the arc of 71°. This gives an approximate speed of 190 m s^{-1}.

From the flow patterns observed throughout the sequence in Figure 2, the observable tip of the arc is controlled by the flows at the poleside edge of the dawn hemisphere cell. The arc is driven on the poleward side by the antisunward flows in the convection throat. The speeds of the tip for each time step range from 0.5 km s^{-1} to a maximum of 1.5 km s^{-1} (the linear fit to the latter part of the upper trace in Figure 7 shows a speed of 1.0 km s^{-1}, assuming a constant latitude of 82°). The maximum measured SuperDARN flow speeds (~835 m s^{-1}) are approximately coincident with the observed maximum DMSP speeds (~2.4 km s^{-1}). The difference in magnitude between SuperDARN and DMSP may be due to differences in the sampling technique and a well-known discrepancy between the two techniques. DMSP has a sampling cadence of 4 s, whereas each SuperDARN pattern is built up over 4 min. However, the location of the peak flows and the speed of the arc tip (from the linear fit to the upper trace in Figure 7) are broadly consistent. By the end of the sequence, the tip of the arc reaches the nightside limit of the dawn convection cell (although this cell appears badly constrained by the SuperDARN potential patterns). Overall, the observations are consistent with the arc being entrained within the surrounding ionospheric flow.

The sequence ends with an increase in brightness of the nightside auroral oval. This indicates the start of a substorm (also implied by the *AL* index of Figure 3). *Pellinen et al.* [1990] noted a substorm leading to the destruction of a TPA; however, the arc in this case would not have been classified as a bending arc. The bending arc disappears as the nightside auroral activity increases.

4. Summary and Conclusions

During a period of southward IMF conditions, a bending arc was observed from a high-altitude position that encompassed a view of the entire Northern Hemisphere polar cap. Polar arcs have been previously attributed to $B_z > 0$ nT dynamics and discussed in the context of arcs that form during prolonged periods of northward IMF. However, we propose a model and show supporting observations, whereby the features of a dayside bending arc are produced by magnetopause reconnection that occurs during IMF southward yet B_y-dominated conditions. The model is used to explain the appearance and subsequent motion of a bending arc on the dayside of the polar cap and does not describe other hook-shaped polar cap phenomena that may occur on the nightside (which appear to be explained by the *Milan et al.* [2005] mechanism, for example, as observed by *Fear and Milan* [2012b]).

The bending arc observed in this case formed on the dayside polar cap before one end, the tip, subsequently detached itself and swung into and across the polar cap region. The base of the arc, the part which remained connected to the auroral oval throughout, moved slowly from the dayside to the nightside of

the polar cap. The arc disappeared on the commencement of a substorm, which was evident from the brightening and expansion of emission seen along the nightside auroral oval.

We have demonstrated that the formation of the bending arc is consistent with the picture of a region of newly created open flux joining the dayside polar cap, following a short burst of magnetic reconnection on the dayside magnetopause, under IMF B_y dominant conditions. SuperDARN flows at the time of the arc are consistent with dayside reconnection. The subsequent redistribution of the entire polar cap to accommodate the newly added open flux, and the convection of the flux within the cap, can explain the motion of the arc, itself associated with a region of open flux, after its formation. The speed of the motion of the arc as it swings into the polar cap is consistent with the flow speeds as measured by two methods: from an orbiting spacecraft (DMSP) and from ground-based radar measurements of the ionosphere (SuperDARN). In addition, the detection of magnetosheath plasma in the region of the bending arc by a DMSP satellite during a high-latitude pass of the polar cap shows that the bending arc occurs on open field lines.

The general reconnection signatures observed in this case are consistent with poleward moving auroral forms that are observed during FTEs. The scenario presented in this paper to explain the formation and movement of bending arcs fits within the established magnetospheric paradigm, and no additional mechanism is necessary. The dominance of the IMF B_y component within the existing magnetospheric model leads to a strongly asymmetrical convection pattern and subsequent redistribution of open flux within the polar cap.

Future observations of the Northern and Southern Hemisphere polar caps will allow the study of all types of polar cap features. This work provides a basis for the future study of the formation and motion of bending arcs in the larger context of the magnetospheric cycle.

Acknowledgments

J.A.C. and S.E.M. gratefully acknowledge support from the STFC consolidated grant ST/K001000/1. R.C.F is supported by STFC Ernest Rutherford Fellowship ST/K004298/1. We also gratefully acknowledge support from the International Space Science Institute (ISSI), for the formation of the International Team on Polar Cap Arcs, where discussion of the present study was initiated. The authors thank George Parks and the Polar UVI team for providing UV images. Solar wind data were obtained from the NASA/GSFC OMNI facility (http://omniweb.gsfc.nasa.gov). We are grateful to the principal investigator of the DMSP SSJ4 instrument for the provision of data regarding the precipitating ions (http://cindispace.utdallas.edu/DMSP/dmsp_data_at_utdallas.html). The DMSP particle detectors were designed by Dave Hardy of AFRL, and the data were obtained from JHU/APL (http://sd-www.jhuapl.edu/Aurora/spectrogram/index.html). The authors thank and acknowledge the anonymous referees for their useful comments that have greatly improved this paper.

Larry Kepko thanks Hermann Opgenoorth and another reviewer for their assistance in evaluating this paper.

References

Berchem, J., and C. T. Russell (1984), Flux transfer events on the magnetopause: Spatial distribution and controlling factors, *J. Geophys. Res.*, *89*, 6689–6703, doi:10.1029/JA089iA08p06689.

Berkey, F. T., L. L. Cogger, S. Ismail, and Y. Kamide (1976), Evidence for a correlation between Sun-aligned arcs and the interplanetary magnetic field direction, *Geophys. Res. Lett.*, *3*, 145–147, doi:10.1029/GL003i003p00145.

Chisham, G., et al. (2007), A decade of the Super Dual Auroral Radar Network (SuperDARN): Scientific achievements, new techniques and future directions, *Surv. Geophys.*, *28*, 33–109, doi:10.1007/s10712-007-9017-8.

Cowley, S. W. H., and M. Lockwood (1992), Excitation and decay of solar wind-driven flows in the magnetosphere-ionosphere system, *Ann. Geophys.*, *10*, 103–115.

Dungey, J. W. (1961), Interplanetary magnetic field and the auroral zones, *Phys. Rev. Lett.*, *6*, 47–48, doi:10.1103/PhysRevLett.6.47.

Dungey, J. W. (1963), Interactions of solar plasma with the geomagnetic field, *Planet. Space Sci.*, *10*, 233–237, doi:10.1016/0032-0633(63)90020-5.

Fasel, G. J. (1995), Dayside poleward moving auroral forms: A statistical study, *J. Geophys. Res.*, *100*, 11,891–11,905, doi:10.1029/95JA00854.

Fear, R. C., and S. E. Milan (2012a), The IMF dependence of the local time of transpolar arcs: Implications for formation mechanism, *J. Geophys. Res.*, *117*, A03213, doi:10.1029/2011JA017209.

Fear, R. C., and S. E. Milan (2012b), Ionospheric flows relating to transpolar arc formation, *J. Geophys. Res.*, *117*, A09230, doi:10.1029/2012JA017830.

Fear, R. C., S. E. Milan, R. Maggiolo, A. N. Fazakerley, I. Dandouras, and S. B. Mende (2014), Direct observation of closed magnetic flux trapped in the high latitude magnetosphere, *Science*, *346*, 1506–1510, doi:10.1126/science.1257377.

Frank, L. A., J. D. Craven, J. L. Burch, and J. D. Winningham (1982), Polar views of the Earth's aurora with Dynamics Explorer, *Geophys. Res. Lett.*, *9*, 1001–1004, doi:10.1029/GL009i009p01001.

Greenwald, R. A., et al. (1995), DARN/SuperDARN: A global view of the dynamics of high-latitude convection, *Space Sci. Rev.*, *71*, 761–796, doi:10.1007/BF00751350.

Gusev, M. G., and O. A. Troshichev (1986), Hook-shaped arcs in dayside polar cap and their relation to the IMF, *Planet. Space Sci.*, *34*, 489–496, doi:10.1016/0032-0633(86)90087-5.

Gussenhoven, M. S. (1982), Extremely high latitude auroras, *J. Geophys. Res.*, *87*, 2401–2412, doi:10.1029/JA087iA04p02401.

Hardy, D. A., L. K. Schmitt, M. S. Gussenhoven, F. J. Marshall, and H. C. Yeh (1984), Precipitating electron and ion detectors (SSJ/4) for the block 5D/Flights 6-10 DMSP (Defense Meteorological Satellite Program) satellites: Calibration and data presentation, *Tech. Rep. AFGL-TR-84-0317*, Air Force Geophys. Lab., Hanscom AFB, Mass.

Ismail, S., and C.-I. Meng (1982), A classification of polar cap auroral arcs, *Planet. Space Sci.*, *30*, 319–330, doi:10.1016/0032-0633(82)90037-X.

Khan, H., and S. W. H. Cowley (1999), Observations of the response time of high-latitude ionospheric convection to variations in the interplanetary magnetic field using EISCAT and IMP-8 data, *Ann. Geophys.*, *17*, 1306–1335.

King, J. H., and N. E. Papitashvili (2005), Solar wind spatial scales in and comparisons of hourly Wind and ACE plasma and magnetic field data, *J. Geophys. Res.*, *110*, A02104, doi:10.1029/2004JA010649.

Kullen, A. (2012), Transpolar arcs: Summary and recent results, in *Auroral Phenomenology and Magnetospheric Processes: Earth and Other Planets, Geophys. Monogr. Ser.,* vol. 197, edited by A. Keiling et al., pp. 69–80, AGU, Washington, D. C., doi:10.1029/2011GM001183.

Kullen, A., and P. Janhunen (2004), Relation of polar auroral arcs to magnetotail twisting and IMF rotation: A systematic MHD simulation study, *Ann. Geophys.*, *22*, 951–970, doi:10.5194/angeo-22-951-2004.

Kullen, A., M. Brittnacher, J. A. Cumnock, and L. G. Blomberg (2002), Solar wind dependence of the occurrence and motion of polar auroral arcs: A statistical study, *J. Geophys. Res.*, *107*, 1362, doi:10.1029/2002JA009245.

Lockwood, M., S. E. Milan, T. Onsager, C. H. Perry, J. A. Scudder, C. T. Russell, and M. Brittnacher (2001), Cusp ion steps, field-aligned currents and poleward moving auroral forms, *J. Geophys. Res.*, *106*, 29,555–29,570, doi:10.1029/2000JA900175.

Milan, S. E., M. Lester, S. W. H. Cowley, J. Moen, P. E. Sandholt, and C. J. Owen (1999a), Meridian-scanning photometer, coherent HF radar, and magnetometer observations of the cusp: A case study, *Ann. Geophys.*, *17*, 159–172, doi:10.1007/s00585-999-0159-5.

Milan, S. E., M. Lester, R. A. Greenwald, and G. Sofko (1999b), The ionospheric signature of transient dayside reconnection and the associated pulsed convection return flow, *Ann. Geophys.*, *17*, 1166–1171, doi:10.1007/s00585-999-1166-2.

Milan, S. E., M. Lester, S. W. H. Cowley, and M. Brittnacher (2000), Convection and auroral response to a southward turning of the IMF: Polar UVI, CUTLASS, and IMAGE signatures of transient magnetic flux transfer at the magnetopause, *J. Geophys. Res.*, *105*, 15,741–15,756, doi:10.1029/2000JA900022.

Milan, S. E., B. Hubert, and A. Grocott (2005), Formation and motion of a transpolar arc in response to dayside and nightside reconnection, *J. Geophys. Res.*, *110*, A01212, doi:10.1029/2004JA010835.

Milan, S. E., J. S. Gosling, and B. Hubert (2012), Relationship between interplanetary parameters and the magnetopause reconnection rate quantified from observations of the expanding polar cap, *J. Geophys. Res.*, *117*, A03226, doi:10.1029/2011JA017082.

Pellinen, R. J., H. E. J. Koskinen, T. I. Pulkkinen, J. S. Murphree, and G. Rostoker (1990), Satellite and ground-based observations of a fading transpolar arc, *J. Geophys. Res.*, *95*, 5817–5824, doi:10.1029/JA095iA05p05817.

Rijnbeek, R. P., S. W. H. Cowley, D. J. Southwood, and C. T. Russell (1984), A survey of dayside flux transfer events observed by ISEE 1 and 2 magnetometers, *J. Geophys. Res.*, *89*, 786–800, doi:10.1029/JA089iA02p00786.

Sandholt, P. E., and C. J. Farrugia (2007), Poleward moving auroral forms (PMAFs) revisited: Responses of aurorae, plasma convection and Birkeland currents in the pre- and postnoon sectors under positive and negative IMF B_y conditions, *Ann. Geophys.*, *25*, 1629–1652, doi:10.5194/angeo-25-1629-2007.

Torr, M. R., et al. (1995), A far ultraviolet imager for the international solar-terrestrial physics mission, *Space Sci. Rev.*, *71*, 329–383, doi:10.1007/BF00751335.

Yeoman, T. K., M. Lester, S. W. H. Cowley, S. E. Milan, J. Moen, and P. E. Sandholt (1997), Simultaneous observations of the cusp in optical, DMSP and HF radar data, *Geophys. Res. Lett.*, *24*, 2251–2254, doi:10.1029/97GL02072.